

Article

A Hurricane Initialization Scheme with 4DEnVAR Satellite Ozone and Bogus Data Assimilation (SOBDA) and Its Application: Case Study

Yin Liu ^{1,2,3,4} ¹ Jiangsu Meteorological Observation Center, Nanjing 210041, China; liuyin200421@163.com² State Key Laboratory of Severe Weather, Chinese Academy of Meteorological Sciences, Beijing 100081, China³ Key Laboratory of Atmosphere Sounding, China Meteorological Administration, Chengdu 610225, China⁴ Key Laboratory of Transportation Meteorology, China Meteorological Administration, Nanjing 210041, China

Abstract: The aim of this study is to joint assimilate the ozone product from the satellite Atmospheric Infrared Sounder (AIRS) and bogus data using the four-dimensional ensemble-variational (4DEnVar) method, and demonstrate the potential benefits of this initialization technique in improving hurricane forecasting through a case study. Firstly, the quality control scheme is employed to enhance the ozone product quality from the satellite AIRS; a bogus sea level pressure (SLP) at the hurricane center is constructed simultaneously based on Fujita's mathematical model for subsequent assimilation. Secondly, a 4DEnVar satellite ozone and bogus data assimilation (SOBDA) model is established, incorporating an observation operator of satellite ozone that utilizes the relationship between satellite ozone and potential vorticity (PV) from the lower level of 400 hPa to the upper level of 50 hPa. Finally, several comparative experiments are performed to assess the influence of assimilating satellite ozone and/or bogus data, the 4DEnVAR method and four-dimensional variational (4D-Var) method, and ensemble size on hurricane prediction. It is found that assimilating satellite ozone and bogus data with the 4DEnVar method concurrently brings about significant alterations to the initial conditions (ICs) of the hurricane vortex, resulting in a more homogeneous and deeper vortex with a larger, warmer, and more humid core as opposed to assimilating only one type of data. As the duration of integration increases, the initial perturbations in the upper levels gradually propagate downwards, giving rise to significant disparities in the hurricane prediction when satellite ozone and/or bogus information is incorporated. The results demonstrate that utilizing the 4DEnVar approach to assimilate both satellite ozone and bogus data leads to the maximum enhancement in reducing track error and central SLP error of hurricane simulation throughout the entire 72 h forecasting period, compared to assimilating a single dataset. Furthermore, comparative experiments have indicated that the performance of 4DEnVar SOBDA in hurricane forecasting is influenced by the ensemble size. Generally, selecting an appropriate number of ensemble members can not only effectively improve the accuracy of hurricane prediction but can also significantly reduce the demand for computational resources relative to the 4D-Var method. This study can also serve as an advantageous technical reference for numerical applications of ozone products from other satellites and hurricane initialization.

Keywords: 4DEnVar; hurricane initialization; satellite ozone; data assimilation

Citation: Liu, Y. A Hurricane Initialization Scheme with 4DEnVAR Satellite Ozone and Bogus Data Assimilation (SOBDA) and Its Application: Case Study. *Atmosphere* **2023**, *14*, 866. <https://doi.org/10.3390/atmos14050866>

Academic Editor: Jimmy Dudhia

Received: 30 March 2023

Revised: 9 May 2023

Accepted: 10 May 2023

Published: 12 May 2023



Copyright: © 2023 by the author. Licensee MDPI, Basel, Switzerland. This article is an open access article distributed under the terms and conditions of the Creative Commons Attribution (CC BY) license (<https://creativecommons.org/licenses/by/4.0/>).

1. Introduction

Ozone is a kind of atmospheric trace gas. It not only has an important impact on the survival of human and surface organisms but also affects the process of atmospheric dynamic, thermodynamic, and radiation across the lower and upper layers of the atmosphere. Since variations in ozone concentration at different heights and latitudes result from the atmospheric flow, ozone is, thus, the passive tracer at the synoptic scale. At early stages, the changes over time in the height of the atmosphere, north–south wind component, and temperature at a pressure level of approximately 300 millibars were discovered to be

closely linked to variations in ozone data from the stations [1,2]. It was found that ozone distributions in the tropopause could be treated as the surrogate for potential vorticity (PV) in the stratospheric and contained the information of meso-scale flow regimes [3,4]. Using Total Ozone Mapping Spectrometer (TOMS) ozone data from 1979–1982, Stout and Rodgers [5] concluded that the tropical cyclone changed the moving direction when its distance from the ozone-rich upper tropospheric trough was approximately 15° latitude. With a linear wave model, Riishøjgaard and Källén [6] found that the correlations between PV and ozone column values were associated with Rossby waves, indicating the possibility of ozone data assimilation in general circulation models. Moreover, the fluctuation of vertically integrated ozone was significantly influenced by the motion of upper-level lows and highs [7]. After analyzing satellite ozone data for many years, Jiang et al. [8] found that the interannual variation of the mid-latitude total ozone column was closely related to atmospheric circulation, which was obviously different from that in the tropics.

In recent years, efforts have been undertaken to utilize ozone information in the study of hurricanes. The eyewall and eye regions of hurricanes exhibited the highest and lowest ozone concentrations, respectively, during intensification, as measured by the National Oceanic and Atmospheric Administration (NOAA) aircraft [9]. Conversely, reduced levels of ozone were observed in both the eyewall and eye regions during weakening [9]. Subsequently, this discovery was further confirmed through a thorough analysis of TOMS data from 1996 to 2003 [10]. Moreover, drawing from the robust association between mean potential vorticity (MPV) and upper level geopotential height within tropical cyclones, the TOMS ozone data were successfully incorporated into a numerical weather prediction (NWP) model to provide a more precise representation of the broader atmospheric conditions surrounding Hurricane Erin (2001) [10–12]. Liu and Zou [13] recently conducted the initial attempt to assimilate Atmospheric Infrared Sounder (AIRS) ozone observations in hurricane prediction. In their study, an ozone assimilation scheme utilizing the four-dimensional variational (4D-Var) was introduced and integrated into the non-hydrostatic mesoscale model version 5 (MM5), considering the link between ozone and MPV for chosen model levels. The aforementioned research indicated that the assimilation of ozone observations had a considerable effect on the accuracy of hurricane track prediction.

Additionally, it was discovered that bogus data assimilation (BDA) with 4D-Var method was a productive technique for initializing the hurricane structure to be in agreement with NWP models and with observations [14–17]. In the first place, the sea level pressure (SLP) bogus is calculated by measured variables obtained from the Tropical Prediction Center (TPC). Subsequently, the initial conditions (ICs) for the numerical model which comply with the equation of atmospheric motion are obtained after the assimilation of SLP bogus [18]. With the advancement of assimilation theory and the utilization of advanced computing systems, it had yielded remarkable outcomes in the combined assimilation of bogus and a wide variety of satellite observations to enhance hurricane forecasting [19–24]. In the past few years, Liu and Zhang [25] upgraded the technique proposed by Liu and Zou [13] to develop a bogus and ozone data assimilation (BODA) scheme using the 4D-Var method. Significant enhancements were observed in the accuracy of hurricane prediction, particularly in the simulation of initial configuration, trajectory, and strength.

However, the 4D-Var method also has some drawbacks. In the first place, the background forecast's fixed covariance matrix is not as efficient in capturing the flow-dependent errors compared to the ensemble Kalman filter techniques [26]. In the second place, the 4D-Var method is extremely time-consuming and labor-intensive, requiring multiple iterations of the tangent linear adjoint model to be operated on the powerful parallel computer, as well as the maintenance and development of these models [27]. The same disadvantages can be observed in the study of Liu and Zhang [25]. To tackle the aforementioned challenges associated with 4D-Var, the notion of ensemble is introduced. Firstly, ensemble utilization enables the 4D-Var process to generate a background error covariance matrix that varies with the flow conditions, which is more effective than the static background error covariance matrix [28,29]. Secondly, ensemble members can be used to calculate the gradi-

ent, thus avoiding the need for an adjoint model [30,31]. In comparison to the ensemble four-dimensional variational (En4DVar) technique, which utilizes the adjoint model during the assimilation execution process, the four-dimensional ensemble-variational (4DEnVar) technique has lower precision but higher assimilation efficiency [32,33]. If the accuracy loss is negligible, 4DEnVar could be a very appealing option [34]. Thus, this paper seeks a proper way to joint assimilate the ozone product from the satellite AIRS and bogus data using the 4DEnVar method, in order to further enhance hurricane forecasting.

The structure of this paper is as follows: Section 2 provides a concise overview of the data and methodology employed in this study. In Section 3, we present an outline of the hurricane case that was analyzed in this investigation, as well as the experiment design. In Section 4, we scrutinize the numerical outcomes obtained from the assimilation experiments and forecast experiments. Lastly, Section 5 offers a recapitulation of the discoveries made in this study.

2. Data and Methodology

2.1. AIRS Ozone Data and Bogus Data

At the present, AIRS is the most cutting-edge hyperspectral infrared atmospheric sensing device, encompassing 2378 radiometric bands across wavelengths spanning from 3.74 μm to 15.4 μm . The ozone information can be accessed from level II and level III products of AIRS. Among them, the level II datasets featuring a nadir ground sample distance of 45 km in its captured imagery include the ozone mixing ratio and total ozone column which are generated twice a day. Numerous studies have demonstrated that ozone data retrieved from AIRS are reliable and can be used for further purposes [35–40]. This study utilizes the level II total ozone column product of the AIRS.

As illustrated in Figure 1, the AIRS ozone distribution of Hurricane Earl is strongly linked to the Geostationary Operational Environmental Satellite (GOES)-13 picture of visible clouds. Previous studies have demonstrated that AIRS ozone product can be a useful tool for understanding the hurricane structure in the vicinity of the tropopause, with higher concentrations in areas of downward air movement and lower concentrations in areas of upward air movement [41–44]. The AIRS data were accessible by 1800 UTC on 1 September 2010, and this time was designated as the model's starting point.

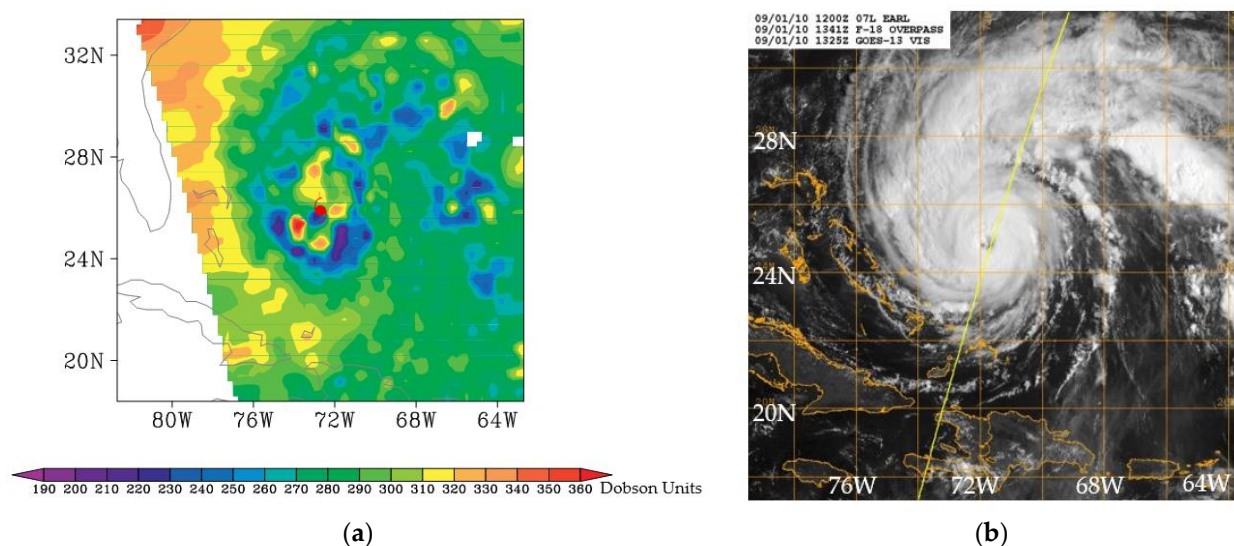


Figure 1. (a) Total ozone column distribution of Hurricane Earl from AIRS at 1800 UTC on 1 September 2010; (b) The picture of visible clouds of Hurricane Earl from GOES-13 at 1325 UTC on 1 September 2010 (<http://www.nrlmry.navy.mil/> (accessed on 20 December 2014)).

It is well known that any data must undergo appropriate quality control before being assimilated into the model, and AIRS data are no exception. However, Liu and Zou [45]

discovered that the majority of AIRS ozone data around the hurricane center were marked as invalid by the official quality control procedure, despite the fact that the observation could be useful. Subsequently, they created a two-step quality control procedure to fulfill the assimilation requirements of satellite ozone, which retained more observations close to the eye of the hurricane than the official quality control procedure. This research employed the quality control scheme developed by Liu and Zou [45] to enhance the data quality of satellite ozone. As Table 1 indicates, the quality control process has significantly enhanced the relationship between ozone data obtained from the AIRS and MPV, and reduced mean error and standard deviation, which facilitates the incorporation of AIRS ozone observation into assimilation processes.

Table 1. Data attributes prior to and following quality control.

	Mean Error (DU)	Standard Deviation (DU)	Correlation Coefficient (AIRS Ozone and MPV)
Prior to quality control	−2.3243	23.3862	0.5428
Following quality control	1.2473	14.2231	0.8801

In addition, a bogus is assimilated to produce a more believable starting vortex at the lower level, while assimilating satellite ozone improves the ICs at the higher level. In this study, a bogus SLP is constructed based on Fujita’s formula for subsequent assimilation [46], and the construction function is shown as follows:

$$P_{\text{bogus}}(d) = P_{\infty} - \frac{(P_{\infty} - P_e)}{[1 + (d/\sqrt{2}D_0)^2]^{1/2}}, \quad d \leq D_{\text{far}}, \tag{1}$$

$$P_{\infty} = \frac{P_{\text{far}}(D_{\text{far}})[1 + (D_{\text{far}}/\sqrt{2}D_0)^2]^{1/2} - P_e}{[1 + (D_{\text{far}}/\sqrt{2}D_0)^2]^{1/2} - 1} \tag{2}$$

where d represents the distance from the eye of the hurricane, P_{∞} denotes the estimated SLP at an extremely distant location, P_e represents the SLP at the eye of the hurricane, P_{far} is the farthest closed isobar, D_0 refers to the distance at which the SLP gradient is the steepest, and D_{far} denotes the radius of P_{far} . It is worth noting that the parameters P_e , P_{far} , and D_{far} can be determined from the observational report of the National Hurricane Center (NHC), while D_0 is derived using the range of wind speeds reaching 34 knots from the center. Figure 2 displays the spatial pattern of SLP bogus for Hurricane Earl, with $P_e = 940.6$ hPa, $P_{\text{far}} = 1008.5$ hPa, $D_{\text{far}} = 374.1$ km, and $D_0 = 162.9$ km at 1800 UTC on 1 September 2010.

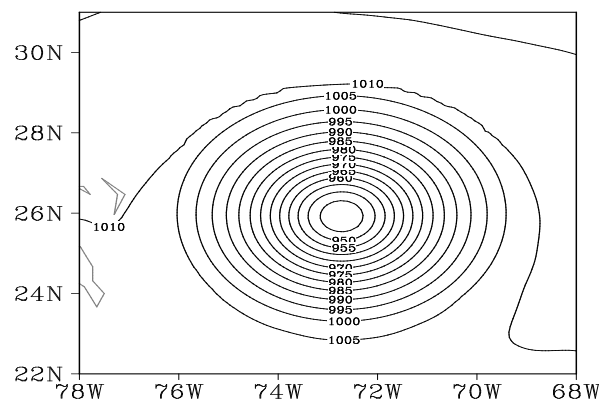


Figure 2. The spatial pattern of SLP bogus at 1800 UTC on 1 September 2010.

2.2. Numerical Model and Observation Operator

Based on the Penn State/National Center for Atmospheric Research (NCAR) non-hydrostatic MM5 [47] and the 4D-Var BODA scheme developed by Liu and Zhang [25], a 4D-EnVar SOBDA model is established in this study. The experiments utilized two model grids (as shown in Figure 3), where the larger grid (D01) consisted of 105×105 points and simulated the broader atmospheric conditions with a horizontal spacing of 45 km, while the smaller grid (D02) consisted of 101×101 points and moved with the hurricane to simulate the more localized atmospheric conditions with a horizontal spacing of 15 km. The vertical direction of model has 27 levels, and the model extends up to a pressure of 50 hPa. Physical parameterizations employed in the model include the Dudhia moisture scheme, the Grell cumulus scheme, and the Blackadar planetary boundary layer scheme. The initial boundary conditions are sourced from NCEP/GFS FNL data at a resolution of 1 degree in both latitude and longitude.

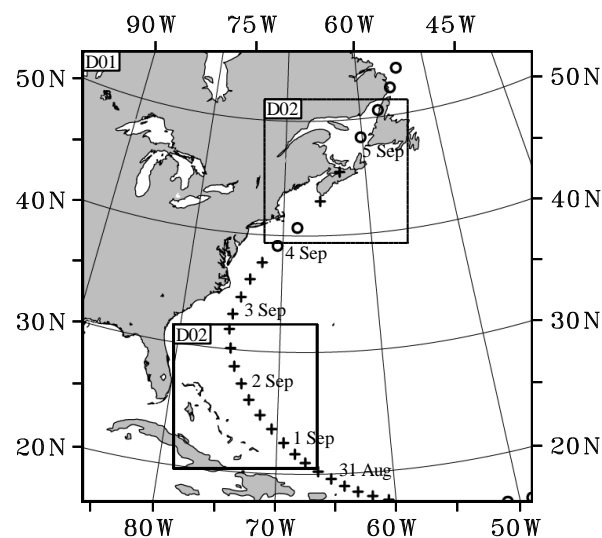


Figure 3. The path of Hurricane Earl, spanning from 0000UTC on 30 August 2010 to 1800UTC on 5 September 2010. The path is indicated by unfilled circles for storms or depressions, as well as cross symbols for hurricanes, with the corresponding dates labeled along its trajectory. Additionally, the image shows the outermost forecast domain D01, which had a resolution of 45 km, along with the inner domains D02, with a resolution of 15 km, that moved along with the hurricane during the 3-day forecast period. One of these domains was positioned at the start of the forecast period, at 1800UTC on 1 September 2010, while the other was located at the end of the forecast period, at 1800UTC on 4 September 2010. (Liu and Zhang [25]).

Assimilating ozone data in NWP models is challenging, as it is not a model variable. In the early days, Jang et al. [11] observed that there was a strong link between ozone measurements from TOMS and MPV in zones between the equator and the poles, which could be expressed as a linear regression model. Then, taking the linear regression model as an observation operator, a procedure for assimilating TOMS total ozone data was developed to enhance hurricane track prediction, following the separation of storm-scale and synoptic-scale features [10,12]. In recent years, the first attempt had been made to assimilate AIRS ozone observations into meso- and micro-scale fields, which had higher spatial and temporal resolutions than TOMS ozone data [13,25]. The following procedures were conducted in their experiments: (1) To confirm the strong correlation, the researchers estimated the relationship between ozone measured by AIRS and MPV within the study area; (2) The correlation coefficient between the ozone observation and PV was computed at each layer of the model ranging from 400 hPa to 50 hPa; (3) Based on the strongest correlation values obtained from step (2), n ($n = 1, 2, 3, \dots, 11$) layers of the model were selected, and an observation operator was created for each layer to be used in the

subsequent assimilation process. One possible formulation for the observation operator is a linear regression model given by

$$TO = a \times PV + b. \tag{3}$$

where a and b are constants that are calculated by analyzing the statistical information on total ozone (TO) and PV (PV). Thus, the total ozone is linked to the model variables through Equation (3). This study adopted the same observation operator and processing steps as Liu and Zhang [25]. Based on the previous conclusion, this study sets n to 5 as the most appropriate value. Table 2 presents the figures of a and b associated with the five layers that were selected.

Table 2. The figures of a and b associated with the five layers that were selected.

Model Layer	a	b
193 hPa ($\sigma = 0.15$)	−1.98	275.54
231 hPa ($\sigma = 0.19$)	−3.62	276.21
269 hPa ($\sigma = 0.23$)	−3.38	276.31
307 hPa ($\sigma = 0.27$)	−3.21	276.47
345 hPa ($\sigma = 0.31$)	−3.33	276.70

2.3. 4D-EnVar Method

The 4D-Var method utilizes dynamic equations to construct the cost function, and then the optimal analysis value is achieved by searching for the cost function’s minimum value with respect to the control variable. The following expression represents the cost function that needs to be minimized [13]:

$$J(x_0) = \frac{1}{2}(x_0 - x_b)^T B_c^{-1}(x_0 - x_b) + \frac{1}{2} \sum_{i=k}^{i=0} [H_i M_{0 \rightarrow i}(x_0) - y_i]^T R_i^{-1} [H_i M_{0 \rightarrow i}(x_0) - y_i]. \tag{4}$$

where x_0 is the state variable at time t_0 , x_b denotes the initial background value at t_0 , B_c^{-1} represents the inverse matrix of the static covariance matrix of background error B , R_i is the covariance matrix of observation error at time t_i , y_i denotes the observations at t_i , M represents the state transition operator, and H_i denotes the observation operator transforming the model domain into the observation domain at t_i . Thus, the cost function’s gradient in relation to x_0 is [26]

$$\nabla J(x_0) = B_c^{-1}(x_0 - x_b) + \sum_{i=k}^{i=0} M_{0 \rightarrow i}^T H_i^T R_i^{-1} [H_i M_{0 \rightarrow i}(x_0) - y_i] \tag{5}$$

where M represents the linearized dynamical system and M^T denotes the adjoint system.

The primary goal of 4D-EnVar is to employ the ensemble to precisely calculate M^T . The state variable’s accumulation from t_0 to t_i is represented by

$$x_i = M_{0 \rightarrow i}(x_0). \tag{6}$$

The reference state at t_0 is named x_0^* . Subsequently, x_0^* is perturbed by adding \tilde{x}_0 :

$$x_i^* + \tilde{x}_i = M_{0 \rightarrow i}(x_0^* + \tilde{x}_0). \tag{7}$$

The first-order Taylor expansion of Equation (7) at x_0^* is expressed as [28]

$$x_i^* + \tilde{x}_i = M_{0 \rightarrow i}(x_0^*) + M_{0 \rightarrow i} \tilde{x}_0 + o(\tilde{x}_0). \tag{8}$$

If $o(\tilde{x}_0)$ is not taken into account, the perturbation at t_i caused by the perturbation at t_0 can be denoted by

$$\tilde{x}_i \approx M_{0 \rightarrow i} \tilde{x}_0. \tag{9}$$

Then, the initial perturbation ensemble \tilde{X}_0 is denoted by [29]

$$\tilde{X}_0 = (\tilde{x}_0^1, \tilde{x}_0^2, \dots, \tilde{x}_0^j), \tag{10}$$

where j denotes the ensemble size. At t_i , the perturbation ensemble \tilde{X}_i can be represented by

$$\tilde{X}_i \approx M_{0 \rightarrow i} \tilde{X}_0. \tag{11}$$

A matrix that describes the covariance of errors across different time periods is defined as [27]

$$B_{ij} = \frac{1}{N-1} \tilde{X}_i \tilde{X}_j^T. \tag{12}$$

Therefore, Equation (11) can be converted to

$$B_{i0} \approx M_{0 \rightarrow i} B_{00}, \tag{13}$$

while $M_{0 \rightarrow i}^T$ satisfies

$$B_{0i} \approx B_{00} M_{0 \rightarrow i}^T, \tag{14}$$

where B_{00} is the B matrix with flow-dependent characteristics. Moreover, a reduction coefficient μ is incorporated to decrease the perturbation at the initial time by a factor of $\sqrt{\mu}$, with the aim of taking into account the accuracy of the adjoint system estimation. Then, the B_e matrix with flow-dependent characteristics is expressed as [30]

$$B_e = \frac{B_{00}}{\mu}. \tag{15}$$

Incorporating B_e results in a new expression for the cost function, as follows [31]:

$$J(\tilde{x}_0) = \frac{1}{2} (x_0^* + \tilde{x}_0 - x_b)^T B_e^{-1} (x_0^* + \tilde{x}_0 - x_b) + \frac{1}{2} \sum_{i=k}^{i=0} [H_i M_{0 \rightarrow i} (x_0^*) + H_i M_{0 \rightarrow i} \tilde{x}_0 - y_i]^T \times R_i^{-1} [H_i M_{0 \rightarrow i} (x_0^*) + H_i M_{0 \rightarrow i} \tilde{x}_0 - y_i] \tag{16}$$

The following expression represents the cost function's gradient in terms of \tilde{x}_0 [34]:

$$\nabla J(\tilde{x}_0) = B_e^{-1} (x_0^* + \tilde{x}_0 - x_b) + \sum_{i=k}^{i=0} M_{0 \rightarrow i}^T H_i^T R_i^{-1} \times [H_i M_{0 \rightarrow i} (x_0^*) + H_i M_{0 \rightarrow i} \tilde{x}_0 - y_i] \tag{17}$$

3. Case Description and Experiment Design

3.1. Case Description

For the convenience of comparison, Hurricane Earl (2010) used in Liu and Zhang [25] is chosen for numerical experiments in the present investigation. On 25 August 2010, Earl formed as a tropical depression and was classified as a tropical storm two days later. At 0000 UTC on 3 August, it underwent intensification and was upgraded to a category 3 hurricane. After 48 h, it continued to strengthen and was reclassified as a category 4 hurricane. According to NOAA data, Earl maintained this level of intensity until 1800 UTC on 1 September, with maximum sustained winds over 225 km/h and a minimum SLP below 930 hPa. At 0000 UTC on 4 September, Earl weakened to a tropical storm before it hit Nova Scotia as a category 1 hurricane later that day. At 0600 UTC on 6 September, it had joined forces with an additional low pressure center situated in the Labrador Sea (Figure 3). This study concentrates on the time frame between 1800 UTC on

1 September 2010 and 1800 UTC on 4 September 2010 when Earl was at its strongest before it made landfall.

3.2. Experiment Design

The impact of assimilating satellite ozone and bogus data regarding the forecast of Hurricane Earl over a period of 72 h is assessed through three 4D-EnVar experiments. “SOBDA” obtains its ICs by assimilating both satellite ozone and bogus data, “BDA” includes only the assimilation of bogus data, and “SODA” includes only the assimilation of satellite ozone observations. Predictions that are initialized with x_b and do not involve data assimilation are denoted as “CTRL”. In three 4D-EnVar experiments, satellite ozone and/or bogus data from 1800 UTC on 1 September 2010 are incorporated into a 4D-EnVar assimilation window of 30 min, with 3 min intervals between assimilations. Furthermore, a set of experiments is carried out to thoroughly compare the disparities between the outcomes of 4D-EnVAR and 4D-Var, and to explore the influence of the number of ensemble members on 4D-EnVAR experiments.

4. Numerical Results

4.1. Initial Structure

Based on NCEP/GFS FNL data, CTRL generates a weak vortex with the center SLP of 984 hPa at the starting point (Figure 4a). As anticipated, the center SLP of BDA or SOBDA fills up quickly in the core area and gradually in the exterior area (Figure 4b,d), exhibiting a horizontal spread that is comparable to that of the SLP bogus (Figure 2). Nevertheless, it is clear that assimilating satellite ozone data alone has a negligible effect on the initial SLP (Figure 4c). Figure 5 displays the cross-sectional view of pressure perturbation across the west–east axis prior to assimilation (CTRL) and pressure perturbation increments after assimilation (BDA, SODA, and SOBDA) through the hurricane center. Similarly, a slight modification is made to the initial pressure perturbation of SODA (Figure 5c), compared with CTRL (Figure 5a). Figure 5b illustrates that BDA induces negative pressure perturbation increments that reach the mid-levels of the troposphere, with magnitudes of approximately -2 to -1 hPa. In contrast to BDA, negative pressure perturbation increments caused by SOBDA are observed across the lower to upper levels, with a maximum value of -18 hPa (Figure 5d). The findings indicate that SOBDA has created a more comprehensive and consistent initial vortex compared to BDA and SODA.

To achieve equilibrium between pressures and wind modifications within the NWP model limit, the temperature fields as well as the humidity fields are also altered during the minimization process of the cost function. The cross-sectional view of the temperature and humidity fields across the west–east axis prior to assimilation (CTRL) and after assimilation (BDA, SODA, and SOBDA) through the hurricane center are shown in Figures 6 and 7. The results indicate that the CTRL simulation (as shown in Figures 6a and 7a) is unable to replicate the deviations in temperature and humidity that are typically observed during the mature phase of a hurricane, due to the lack of observations in the hurricane circulation over the open ocean. Notably, considerable adjustments are made to the temperature fields as well as the humidity fields of a hurricane in BDA and SOBDA. Moreover, Figures 6 and 7 show the temperature increments and specific humidity increments in BDA (Figures 6b and 7b), SODA (Figures 6c and 7c), and SOBDA (Figures 6d and 7d) which are represented by the shaded areas. The temperature elevation above the hurricane center in BDA is limited to 3 K between 600 hPa and 200 hPa (Figure 6b), which reveals a lack of strength in the warm core. Within the lower levels of the atmosphere in the BDA simulation, the most significant increase in specific humidity is observed at 750 hPa, with a rise of 6 g kg^{-1} as depicted in Figure 7b. The warm core of BODA is more pronounced than that of BDA, as shown by the temperature above the hurricane center which increases up to 9 K around 250 hPa and 400 hPa (Figure 6d). It is noteworthy that the robust warm core is in agreement with the strong perturbation pressure that is presented in Figure 5d. Meanwhile, the BODA simulation exhibits a substantial increase in specific humidity between 900 hPa

and 550 hPa, with the most significant rise of 10 g kg^{-1} occurring in the vicinity of 750 hPa (Figure 7d). It is also noticed that the initial vortex of SODA does not exhibit the warm and moist core that is present in the initial vortex of BDA and SOBDA (Figures 6c and 7c). The temperature fields as well as the humidity fields in SODA are similar to CTRL.

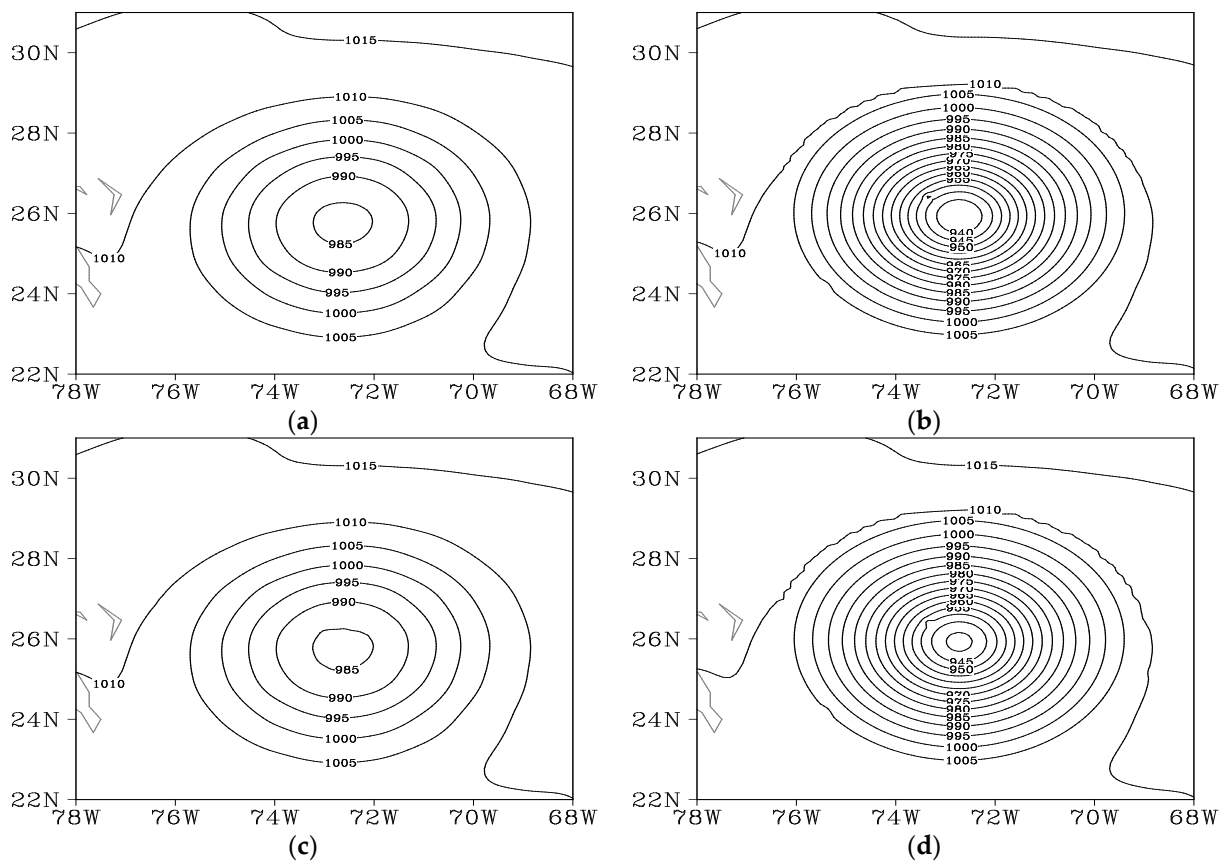


Figure 4. The spatial distribution of SLP at the starting point: (a) CTRL; (b) BDA; (c) SODA; (d) SOBDA. The SLP contour lines are spaced at intervals of 5 hPa.

As satellite ozone and PV are closely related, this study integrates AIRS ozone data into the hurricane simulation, which necessitates an evaluation of PV increments subsequent to data assimilation. Figure 8 illustrates the cross-sectional view of PV across the west–east axis prior to assimilation (CTRL) and PV increments after assimilation (BDA, SODA, and SOBDA) through the hurricane center. The application of the BDA procedure leads to an elevation in PV above the hurricane center, as indicated by the data presented in Figure 8b. Specifically, this increase occurs within the range of 950 hPa to 300 hPa, with the highest observed increase being 3 PVU at approximately 600 hPa. In contrast, SODA mainly alters the ICs of PV in the upper troposphere, leading to a 5 PVU increase near 250 hPa as shown in Figure 8c. As expected, the height range of the PV increment in SODA is basically consistent with the height range of assimilating AIRS ozone data. In SOBDA, the combined assimilation of both satellite ozone and bogus data makes significant changes in the entire PV field (Figure 8d). One notable characteristic is the significant increase in PV at both the lower and upper levels, with an increase of up to approximately 10 PVU. However, a slight decrease in PV is observed near 450 hPa.

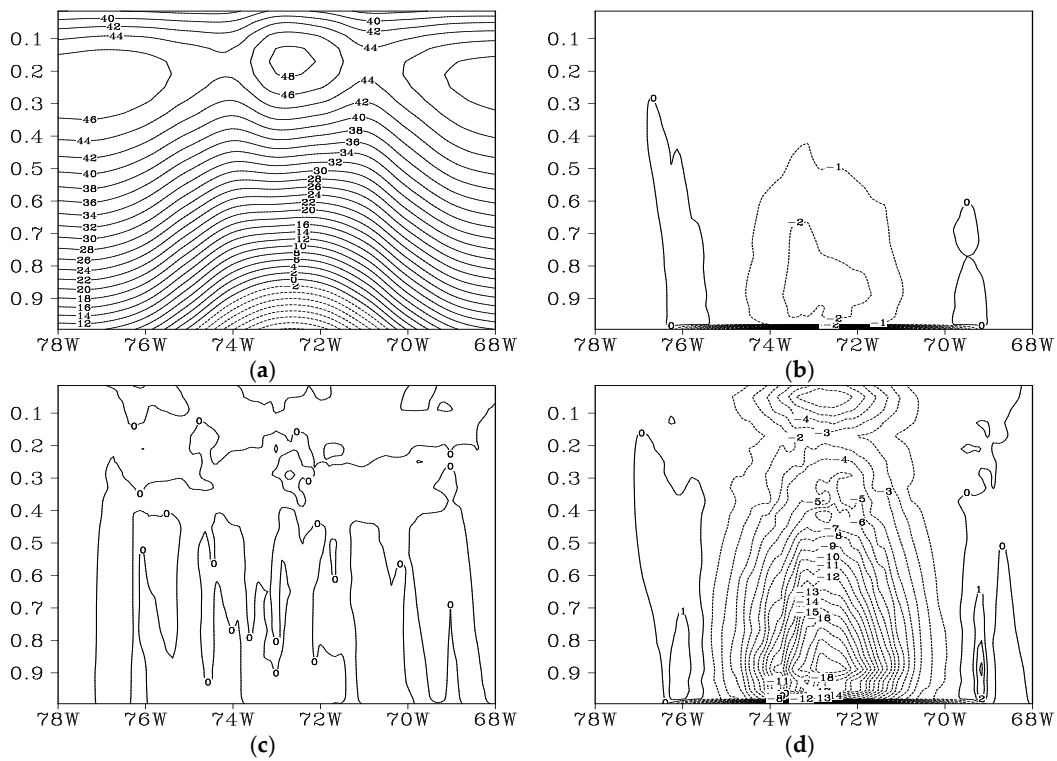


Figure 5. The cross-sectional view of pressure perturbation across the west–east axis prior to assimilation ((a) CTRL) and pressure perturbation increments after assimilation ((b) BDA; (c) SODA; (d) SOBDA) through the hurricane center. The contour lines are spaced at different intervals: (a) 2 hPa; (b–d) 1 hPa.

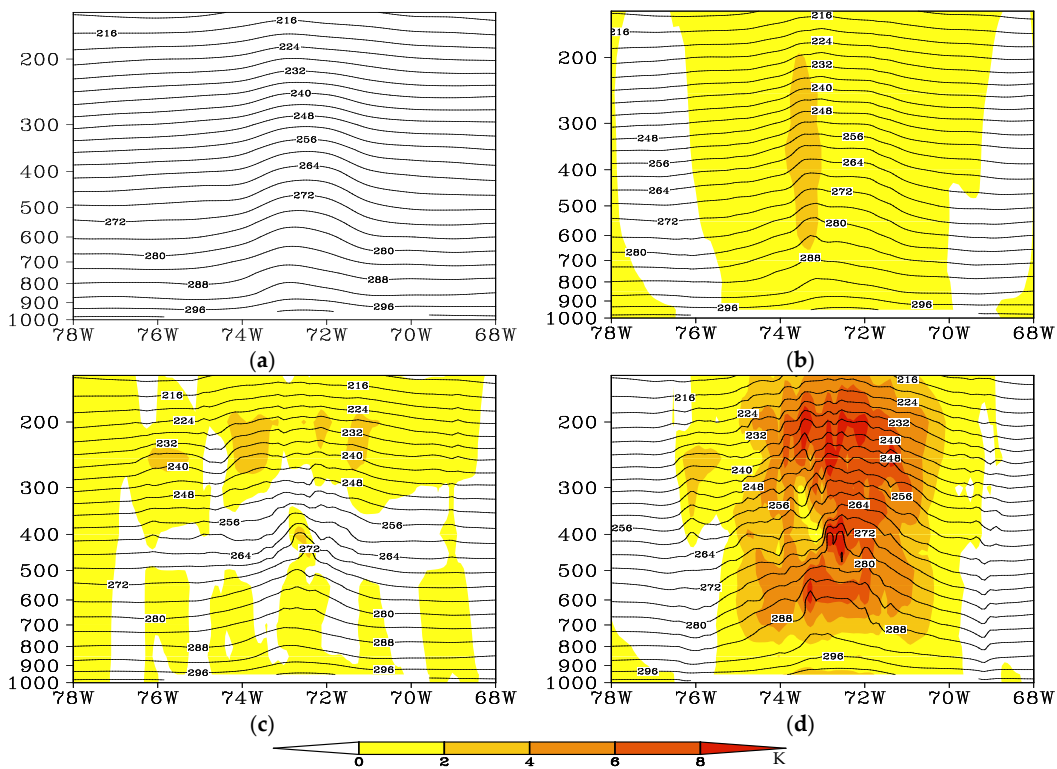


Figure 6. The cross-sectional view of the temperature (solid line) across the west–east axis prior to assimilation ((a) CTRL) and after assimilation ((b) BDA; (c) SODA; (d) SOBDA) through the hurricane center, with its increments (shading). The temperature contour lines are spaced at intervals of 4 K.

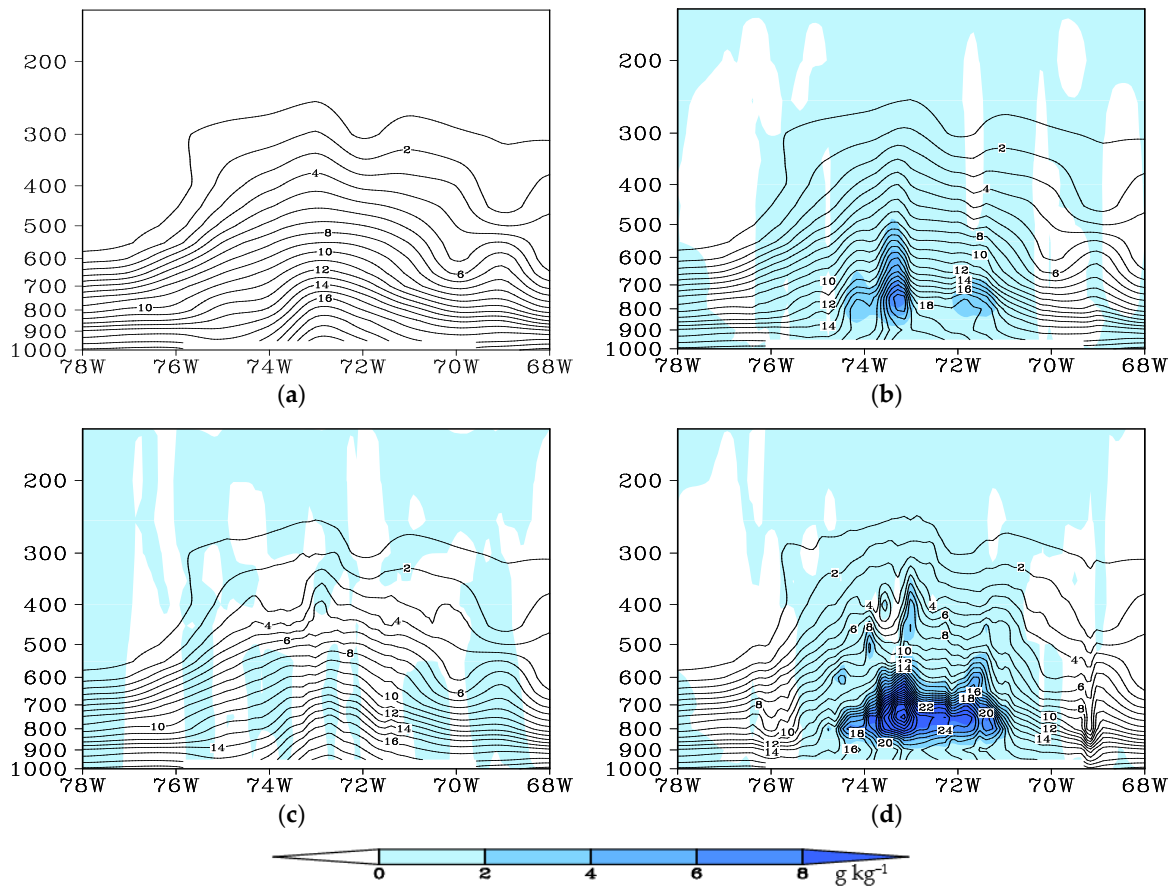


Figure 7. The cross-sectional view of the specific humidity (solid line) across the west–east axis prior to assimilation ((a) CTRL) and after assimilation ((b) BDA; (c) SODA; (d) SOBDA) through the hurricane center, with its increments (shading). The specific humidity contour lines are spaced at intervals of 1 g kg^{-1} .

The aforementioned results demonstrate that the mature hurricane structure generated by SOBDA is more realistic than the ones generated by BDA and SODA. It is worth noting that the increment of SOBDA is not a simple sum of the increment of BDA and the increment of SODA. The main reason is that the 4DnVar method seeks the optimal ICs under the constraint of the NWP model, so the initial model fields are dynamically and physically consistent. These modifications of the upper levels using AIRS ozone data, as well as the lower levels with bogus data, result in a stronger intensity prediction of a hurricane.

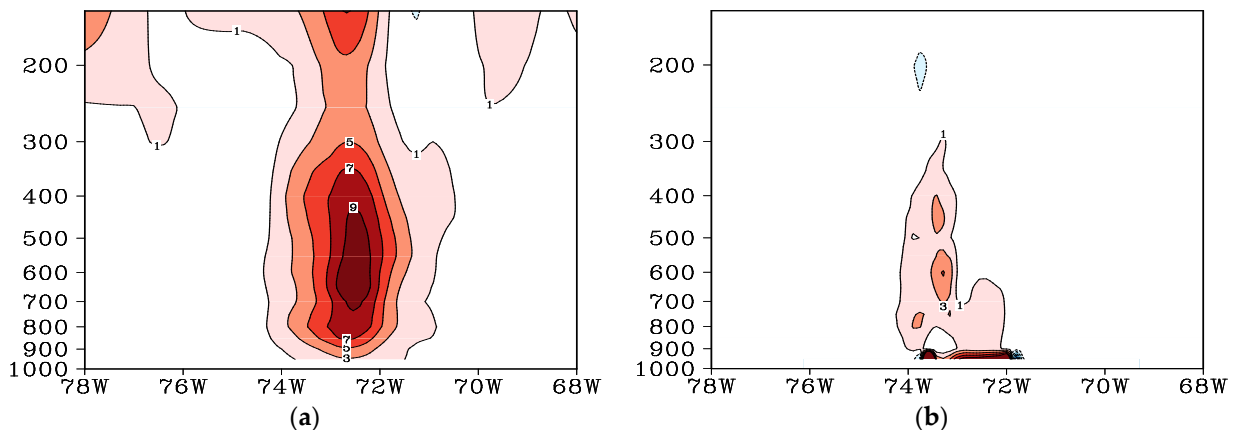


Figure 8. Cont.

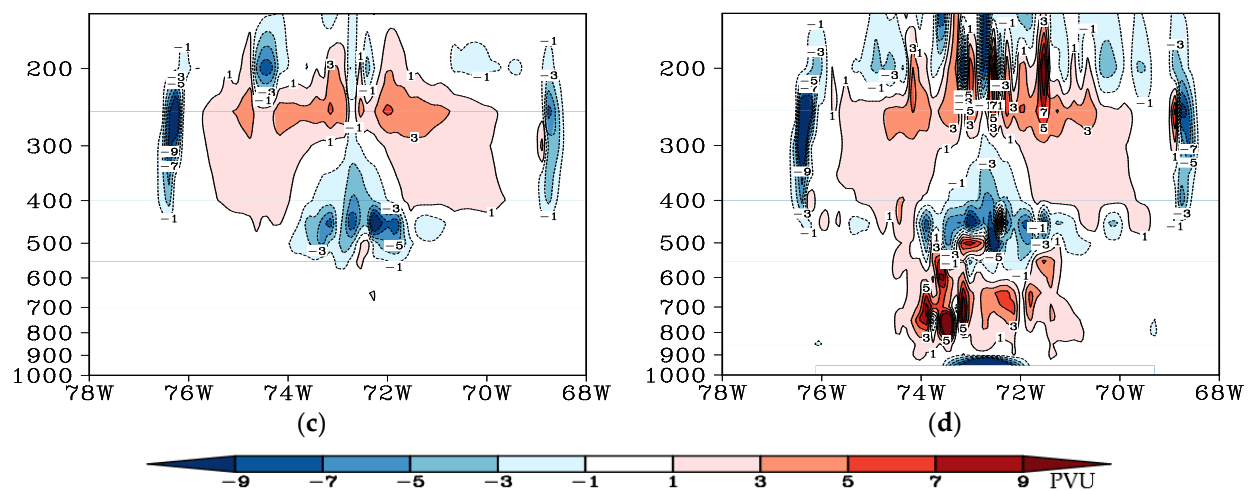


Figure 8. The cross-sectional view of PV across the west–east axis prior to assimilation ((a) CTRL) and PV increments after assimilation ((b) BDA; (c) SODA; (d) SOBDA) through the hurricane center. The PV and its increment contour lines are spaced at intervals of 2 PVU.

4.2. Track and Intensity

In Figure 9a, the simulated hurricane tracks from CTRL, BDA, SODA, and SOBDA beginning at 1800 UTC on 1 September 2010 are depicted, with the observed best track of Unisys (OBS) presented for reference. More details can be found in Appendix A Table A1. It has been noted that Earl initially proceeded in a northwesterly direction, after which it made a sudden change in course and moved towards the northeast 24 h later. As no data was assimilated into the initial model fields with a cold start, CTRL’s prediction of the hurricane track is seen to be on the east side of OBS, resulting in a rapid increase in track error after the initial time and a postponement in the hurricane’s arrival on land with an approximate positional discrepancy of 255 km (Figure 9b). In comparison to CTRL, other experiments assimilating satellite ozone and/or bogus data yield varying levels of improvement in the hurricane’s track simulation. In addition, SOBDA demonstrates a more substantial enhancement in the hurricane’s track prediction compared to BDA and SODA throughout the entire 72 h prediction timeframe, with the track deviation staying under 130 km and the hurricane’s landfall location being nearer to OBS. It is evident that the disparities between the four prediction tracks are minimal during the initial 9 h, but become much more pronounced afterwards.

Figure 10 illustrates the time-varying center SLP and its error from CTRL, BDA, SODA, and SOBDA, with the observation of Unisys (OBS) provided for comparison. If bogus data are not assimilated, the predicted center SLP variations of Hurricane Earl by CTRL and SODA exhibit a comparable pattern that is not able to accurately reflect the hurricane’s intensity. On the other hand, BDA and SOBDA not only produce an initial center SLP of approximately 940 hPa, which is nearly identical to OBS, but also generate powerful hurricanes with a center SLP lower than 930 hPa. Furthermore, the center SLP error from SOBDA initialized with assimilating satellite ozone and bogus data is significantly smaller compared to BDA, except for the first 6 h. It is probable that the spinup issue, observed during the integration of SOBDA, as shown by the sudden jump in center SLP within the first 6 h in Figure 10a, is caused by the implementation of a solitary domain for data assimilation and two nested domains for hurricane prediction.

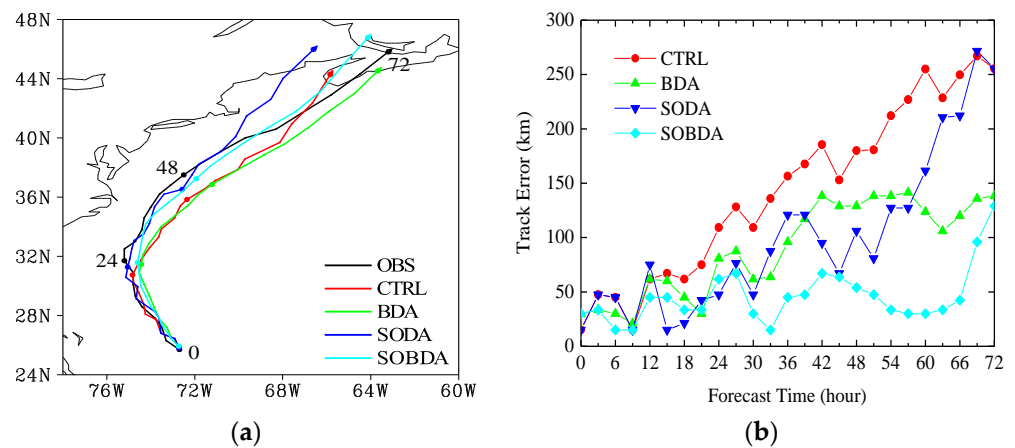


Figure 9. (a) The simulated hurricane tracks from CTRL, BDA, SODA, SOBDA, and the observed best track of Unisys (OBS) beginning at 1800 UTC on 1 September 2010, with the forecast hours marked along the tracks. The hurricane centers at 0 h, 24 h, and 48 h are marked with dots, and the hurricane centers at 72 h are marked with arrows. (b) Track error of CTRL, BDA, SODA, and SOBDA throughout the entire 72 h prediction timeframe.

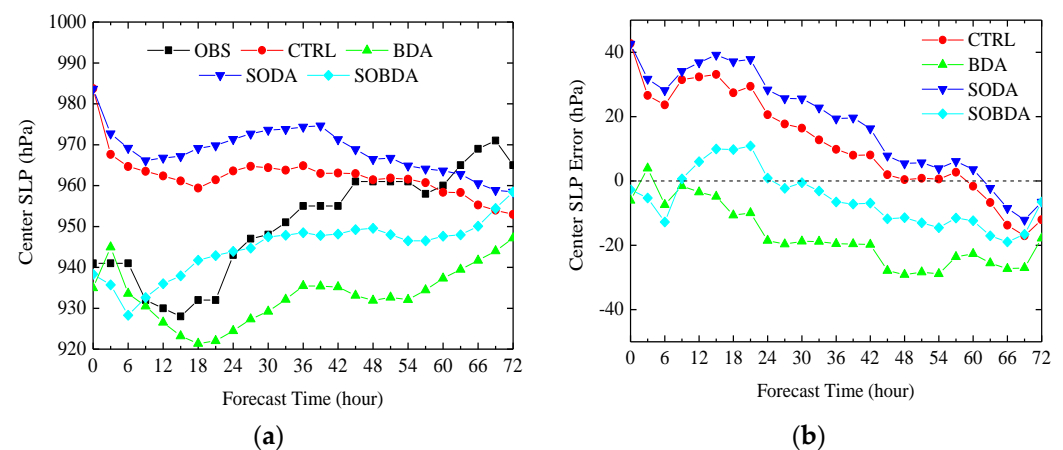


Figure 10. The time-varying center SLP (a) and the center SLP error (b) of CTRL, BDA, SODA, and SOBDA throughout the entire 72 h prediction timeframe, with the observation of Unisys (OBS).

The results presented above suggest that incorporating both satellite ozone and bogus data can lead to a notable enhancement in the simulation of Hurricane Earl’s track and intensity. What leads to the differences while simulating Hurricane Earl? Section 4.3 provides a detailed analysis of the influence of satellite ozone and bogus data on the simulated structures.

4.3. Causes of Simulated Differences

It is noteworthy to look into the hurricane structures after 9 h of integration as the alterations in track and intensity predictions from CTRL, BDA, SODA, and SOBDA become apparent at that moment (Figures 9 and 10). The spatial distribution of SLP from CTRL, BDA, SODA, and SOBDA after 9 h of integration is illustrated in Appendix A Figure A2. It is found that the spatial distribution of SLP in SOBDA is comparable to that of BDA, featuring a reduced central SLP in comparison to CTRL. Nonetheless, the hurricane intensity in the SODA simulation is marginally lower compared to that in CTRL. Appendix A Figure A3 displays the cross-sectional view of pressure perturbation across the west–east axis from CTRL and pressure perturbation increments from BDA, SODA, and SOBDA through the hurricane center. It is noteworthy that, despite the initial pressure perturbation being weak in BDA (Figure 5b), the simulated intensity of pressure perturbation after 9 h of adjustment

is considerably stronger than that in SOBDA. After 9 h of integration, a comparable trend can be observed in the vertical temperature distribution from both BDA and SOBDA simulations, passing through the hurricane center, as illustrated in Figure 11b,d. Moreover, the increase in specific humidity in SOBDA is still larger than that in BDA, especially in the lower troposphere (Figure 12b,d). It is also worth noticing that the SODA simulation exhibits a weaker vortex, as depicted in Appendix A Figure A2, which is consistent with the weaker positive increments of pressure perturbation (Appendix A Figure A3).

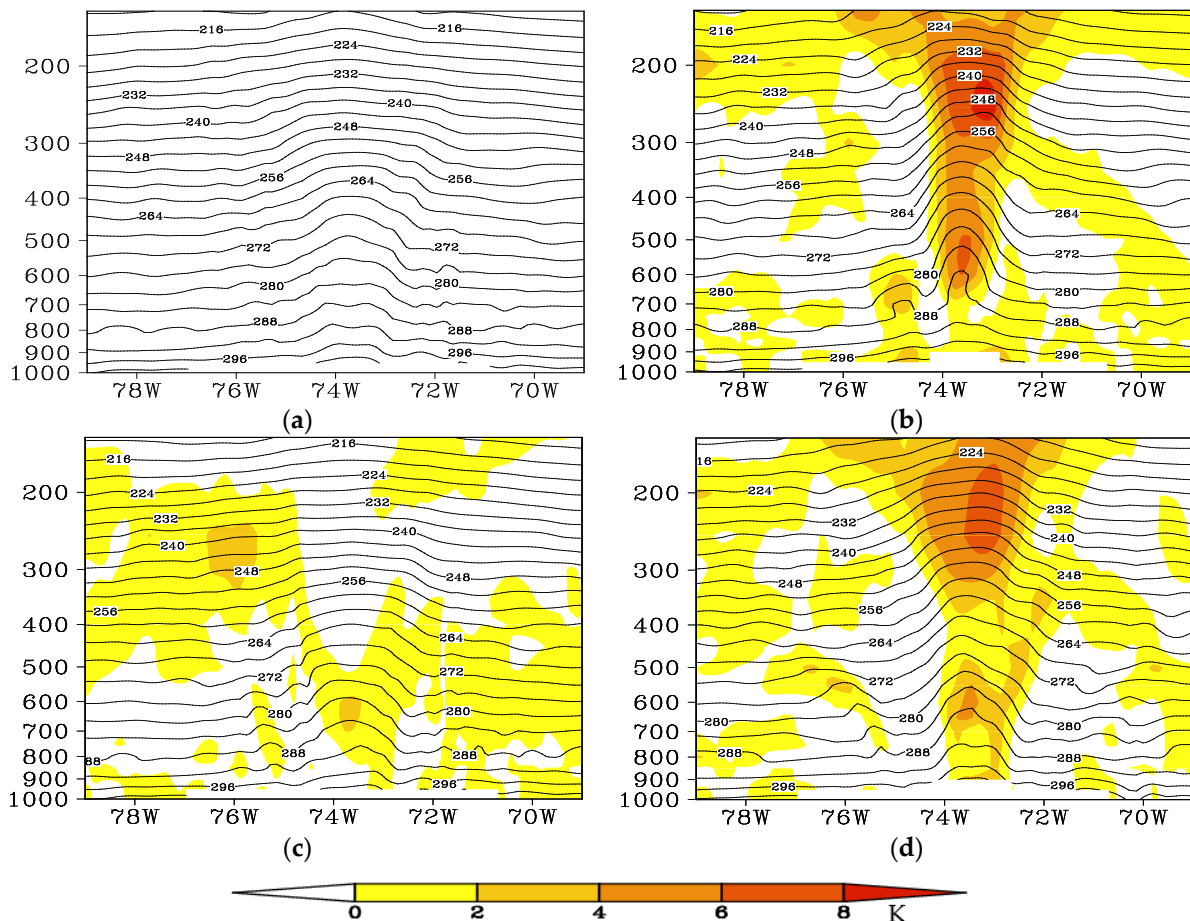


Figure 11. Same as Figure 6, but for the temperature and its increments at the 9 h mark of integration. (a) CTRL; (b) BDA; (c) SODA; (d) SOBDA.

Figure 13 displays the cross-sectional view of PV from CTRL and PV increments from BDA, SODA, and SOBDA through the hurricane center, after 9 h of integration. Despite the fact that assimilating satellite ozone observations at the initial time appears to have a greater influence on the distribution of PV in the vicinity of the tropopause (Figure 8c), the PV differences between SODA and CTRL extend to the lower levels at the 9 h mark of integration (Figure 13c). This is mainly attributed to the increased visibility of diabatic effects and the tropopause dropping to lower levels after a period of model integration. Contrary to the decrease in PV in SODA, BDA experiences a significant increase of PV from the lower to the upper layers (Figure 13b). In contrast to BDA, the addition of AIRS ozone data in SOBDA generates an adjustment after 9 h integration that affects the PV anomaly between 900 hPa and 200 hPa (Figure 13d). As such, the intensified PV anomaly in the lower levels may be one of the causes for the model’s propensity to overpredict the strength of the hurricane during the subsequent simulation of BDA.

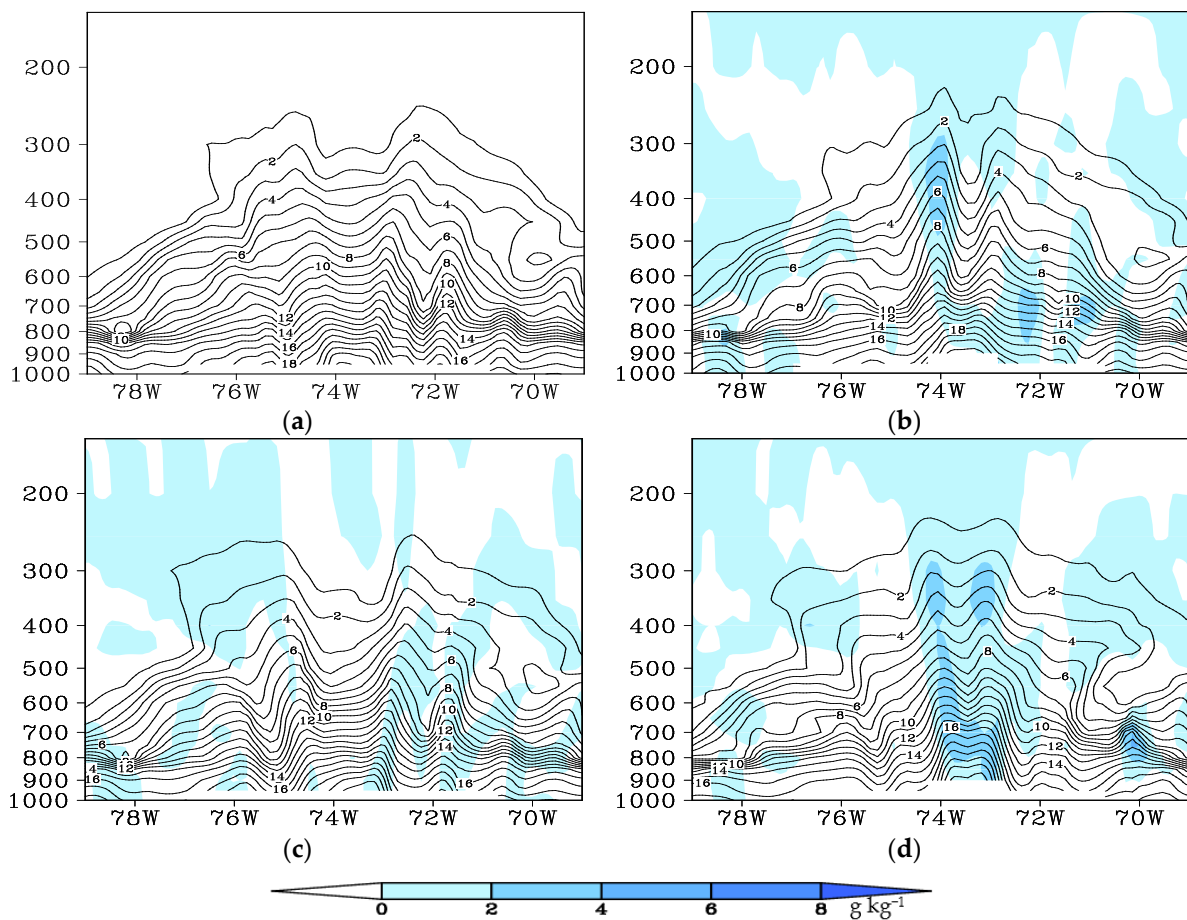


Figure 12. Same as Figure 7, but for the specific humidity and its increments at the 9 h mark of integration. (a) CTRL; (b) BDA; (c) SODA; (d) SOBDA.

Hurricane motion can be approximated by a mass-weighted deep layer-mean flow field, which is generally better than single-level steering [48,49]. The environmental steering flows can be approximated by the mean flows near the hurricane center [50,51]. Therefore, the steering flows in this study are calculated between 850 and 300 hPa in the hurricane center area with a radius of 500 km. Figure 14 shows the zonal and meridional components of the steering flows from CTRL, BDA, SODA, and SOBDA throughout the entire 72 h prediction timeframe. It is found that the zonal component of the steering flows from CTRL, BDA, SODA, and SOBDA first decreased, and then increased during the simulation (Figure 14a), consistent with the simulated motion feature as shown in Figure 9a. Moreover, the zonal component of the steering flows from SODA and SOBDA during 12–36 h is smaller than that from CTRL, resulting in a westward track during the simulation. Figure 14b indicates that the difference in the meridional component of the steering flows from CTRL, BDA, SODA, and SOBDA is obvious after 36 h. In particular, the meridional component of the steering flows from SOBDA is greater than that from CTRL, BDA, and SODA during 42–69 h, while less than that from CTRL and SODA after 69 h, resulting in the meridional difference of the track.

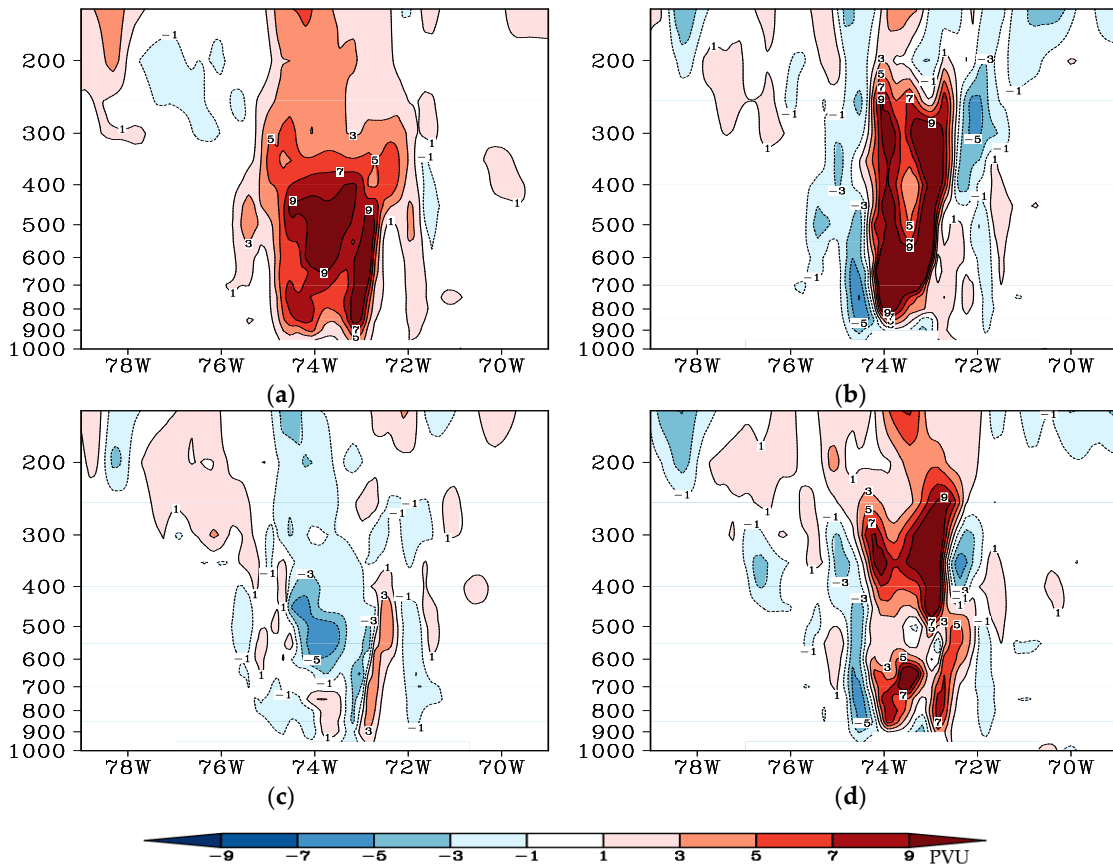


Figure 13. Same as Figure 8, but for the PV and its increments at the 9 h mark of integration. (a) CTRL; (b) BDA; (c) SODA; (d) SOBDA.

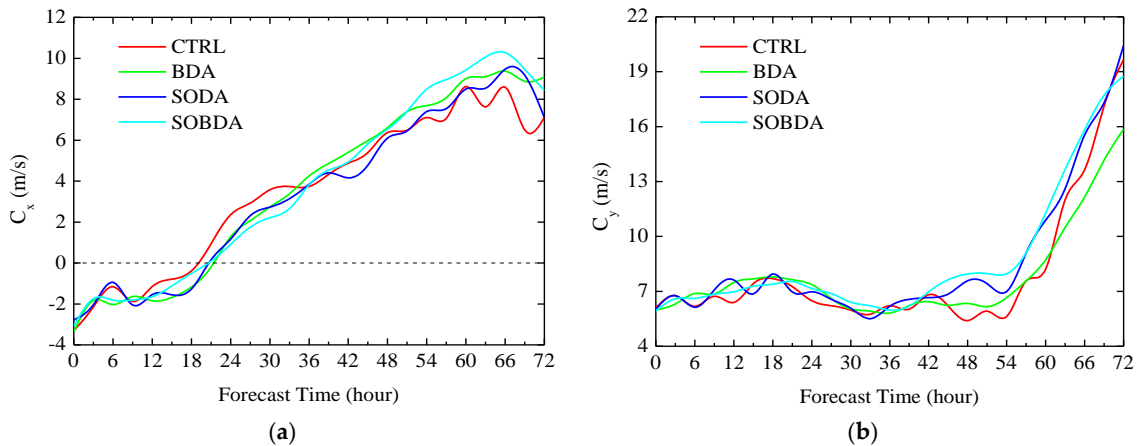


Figure 14. Zonal (a) and meridional (b) components of the steering flows from CTRL, BDA, SODA, and SOBDA throughout the entire 72 h prediction timeframe.

It is reasonable to conclude that assimilating satellite ozone data or/and bogus data will alter the initial structure of the hurricane, then the simulated structure of hurricane and large-scale environmental fields (such as steering flows) will gradually be adjusted as the model is integrated, ultimately leading to differences in the forecast of the hurricane’s track and intensity. Assimilating satellite ozone observations and assimilating bogus data are mutually beneficial and the joint implementation of the two assimilation schemes can bring about a structure of a simulated hurricane that is more accurate and true-to-life as the numerical integration continues. Following the assimilation with a single type of data, the simulation is likely to overestimate the hurricane intensity from BDA as well as

underestimate the hurricane intensity from SODA. The combination of satellite ozone and bogus data in SOBDA allows for all model fields to be adjusted reasonably, leading to a substantial enhancement in forecasting the path and strength of a hurricane. Furthermore, this study also indicates the vital importance of an accurate initial structure in hurricane numerical prediction.

4.4. Impacts of Ensemble Size

In general, increasing the size of the ensemble leads to a decrease in sampling error. Nevertheless, the ensemble size is usually restricted due to computational cost constraints. Therefore, it is essential to scrutinize the effect of the ensemble size on the assimilation and simulation. The same model parameters as those in Section 2.2 are adopted in this section, and experiments are conducted with five different ensemble sizes of 10, 100, 200, 300, and 500. Since the same hurricane case as Liu and Zhang [25] is employed in this study, the experimental results of the 4DEnVAR and 4D-Var methods can also be compared comprehensively. Figure 15 depicts mean track error, mean center SLP error, and computational expense of initialization of the five 4DEnVAR experiments with ensemble sizes of 10, 100, 200, 300 and 500, as well as the 4D-Var experiment from Liu and Zhang [25]. It is observed that as the number of ensemble members increases, the mean track error of each 4DEnVAR experiment for hurricane track forecasting decreases gradually; however, when the number of ensemble members exceeds 200, the improvement of the hurricane track forecast is minimal. In comparison to the 4D-Var experiment, the mean track error of each 4DEnVAR experiment for hurricane track forecasting is decreased to varying extents. In terms of the hurricane intensity forecast, the mean center SLP errors of 4DEnVAR and 4D-Var experiments are similar, both of which present the issue of overestimation. Compared to the others, the 4DEnVAR experiment with 300 ensemble members shows the most significant improvement in the hurricane intensity forecast. It is worth noting that the computation time for the hurricane initialization of each 4DEnVAR experiment is much lower than that of the 4D-Var experiment, with a decrease of more than 50%, especially for the 4DEnVAR experiment with 300 ensemble members which exhibits the highest computing efficiency. Therefore, when utilizing the 4DEnVAR method to joint assimilate satellite ozone and bogus data, an appropriate number of ensemble members should be selected to significantly improve the hurricane prediction and spend a reasonable amount of computing time.

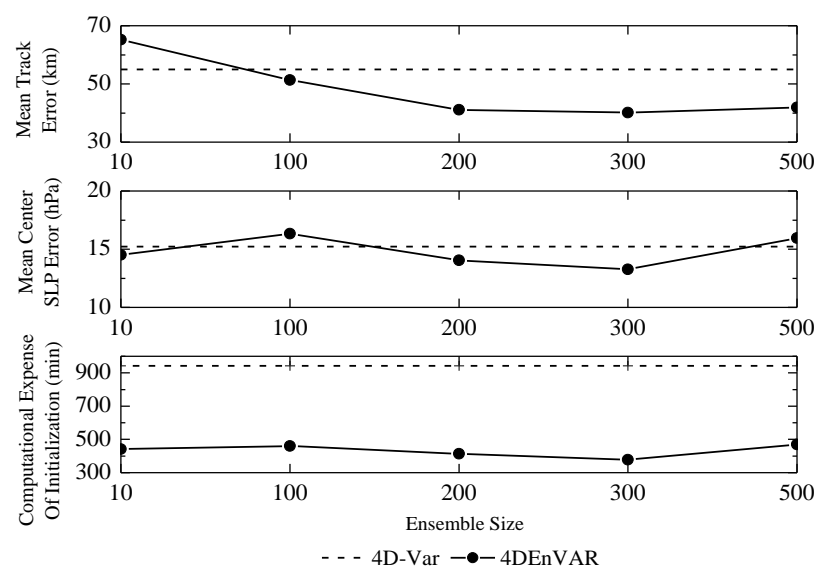


Figure 15. Mean track error, mean center SLP error, and computational expense of initialization of the 5 4DEnVAR experiments with ensemble sizes of 10, 100, 200, 300, and 500, as well as the 4D-Var experiment from Liu and Zhang [25].

5. Summary

A major hurdle in forecasting the path and strength of a hurricane is establishing the initial structure of a hurricane in the open ocean with limited observations. This study endeavors to joint assimilate satellite ozone and bogus data based on the 4D-EnVar method, with a case study illustrating how this initialization scheme could enhance hurricane prediction. To assess the results, four experiments are undertaken: three with the 4D-EnVar assimilation of satellite ozone and/or bogus data and one without. Furthermore, a comprehensive set of experiments have been performed to thoroughly compare the disparities between the outcomes of 4D-EnVAR and 4D-Var, and to investigate how the ensemble size impacts 4D-EnVAR experiments. To sum it up, the following can be noted:

- (1) By assimilating bogus data, the ICs of SLP, pressure perturbation, specific humidity, and PV primarily in the lower atmospheric layers are altered, resulting in a slight intensification of Hurricane Earl's warm core. Assimilating satellite ozone observations has minimal influence on the ICs, except for the PV pattern in the vicinity of the tropopause. Nonetheless, the assimilation of both satellite ozone and bogus data induces notable alterations in the ICs, extending from the lower to the upper layers. This leads to a more extensive, warmer, and moister core of Hurricane Earl, resulting in a more profound and evenly distributed initial vortex, compared to the scenario where only one type of data is assimilated.
- (2) Changes to the lower levels have a greater effect on hurricane development than modifications to the upper levels. As the integration time passes, the perturbations in the upper levels spread to the lower levels, leading to large discrepancies in the forecasts when satellite ozone and/or bogus data are assimilated. The assimilation of both satellite ozone and bogus data provides a more comprehensive and precise depiction of the hurricane structure features, surpassing the accuracy achieved by assimilating only one type of data or not performing any assimilation. Consequently, the implementation of the SOBDA scheme yields a significant improvement in the accuracy of the hurricane track and intensity forecasts during subsequent numerical simulations.
- (3) With the 4D-EnVar method, hurricane prediction is found to be much more sensitive to the ensemble size. By using the 4D-EnVAR method to joint assimilate satellite ozone and bogus data with an appropriate ensemble size, it is possible to significantly enhance hurricane prediction while still consuming a manageable amount of computer resources compared to the 4D-Var method.

This study can provide valuable references for hurricane initialization and numerical applications of ozone data from other satellites. While acknowledging the potential of the new scheme developed in this study, one case study is still insufficient. It is important to gather more case studies in the future in order to arrive at a more comprehensive understanding of its performance. Additionally, there is still room for further improvements of the new scheme. For example, the assimilation of bogus, AIRS ozone, and other satellite data (e.g., the Advanced TIROS Operational Vertical Sounder (ATOVS) microwave data and satellite cloud-derived wind) may further improve the initialization and forecast of hurricanes.

Funding: This research was funded by the Open Grants of the State Key Laboratory of Severe Weather (2020LASW-B11), the Joint Research Project for Meteorological Capacity Improvement (22NLTSY009), the Key Scientific Research Projects of Jiangsu Provincial Meteorological Bureau (KZ202203), the fund of "Key Laboratory of Atmosphere Sounding, CMA" (2021KLAS01M), and the Innovation and Development Project of China Meteorological Administration (CXFZ2023J022).

Data Availability Statement: The data are available upon reasonable request from the author of the paper.

Conflicts of Interest: The author declares no conflict of interest. The funders had no role in the design of the study; in the collection, analyses, or interpretation of data; in the writing of the manuscript; or in the decision to publish the results.

Appendix A

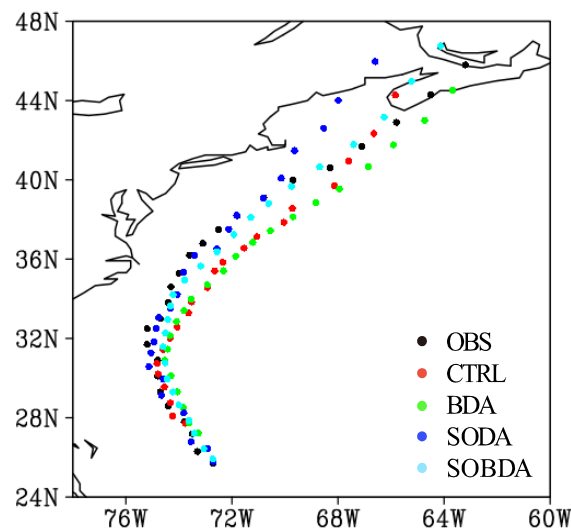


Figure A1. The simulated hurricane tracks from CTRL, BDA, SODA, SOBDA, and the observed best track of Unisys (OBS) beginning at 1800 UTC on 1 September 2010. The hurricane centers are marked with dots at 3 h intervals.

Table A1. The hurricane center location at 3 h intervals from CTRL, BDA, SODA, SOBDA, and the observed best track of Unisys (OBS) beginning at 1800 UTC on 1 September 2010 (LON denotes longitude, the unit is °W; LAT represents latitude, the unit is °N).

Forecast Hours	OBS		CTRL		BDA		SODA		SOBDA	
	LON	LAT								
0	72.70	25.70	72.71	25.79	72.72	25.92	72.71	25.79	72.72	25.92
3	73.30	26.30	72.91	26.44	73.06	26.43	72.91	26.44	73.06	26.43
6	73.50	27.20	73.54	26.80	73.27	27.22	73.54	26.80	73.42	27.21
9	73.80	27.80	73.76	27.72	73.61	27.73	73.63	27.86	73.63	27.86
12	74.40	28.60	74.25	28.09	73.84	28.52	73.81	28.25	74.00	28.64
15	74.70	29.30	74.32	28.75	74.06	29.31	74.66	29.13	74.22	29.30
18	74.80	30.10	74.55	29.55	74.30	30.11	74.59	29.95	74.44	29.96
21	74.80	30.90	74.78	30.21	74.53	30.90	75.13	30.58	74.52	30.77
24	75.20	31.70	74.83	30.74	74.43	31.46	75.05	31.27	74.60	31.58
27	75.20	32.50	74.59	31.44	74.34	32.14	74.95	31.83	74.51	32.27
30	74.70	33.00	74.33	32.01	74.09	32.85	74.86	32.52	74.42	32.96
33	74.40	33.80	74.06	32.57	73.81	33.41	74.76	33.07	74.33	33.65
36	74.30	34.60	73.64	33.29	73.54	33.98	74.32	33.52	74.22	34.21
39	74.00	35.30	73.52	33.84	72.93	34.70	74.06	34.22	73.79	34.93
42	73.60	36.20	72.92	34.57	72.32	35.42	73.83	35.34	73.18	35.65
45	73.10	36.80	72.65	35.41	71.86	36.14	73.40	36.19	72.56	36.38
48	72.50	37.50	72.35	35.84	71.21	36.85	72.57	36.52	71.93	37.24
51	71.80	38.20	71.54	36.56	70.55	37.43	72.12	37.51	71.29	38.10
54	70.80	39.10	71.06	37.13	69.70	38.14	71.82	38.21	70.62	38.81
57	69.70	40.00	70.04	37.86	68.84	38.85	70.81	39.08	69.76	39.67
60	68.30	40.60	69.72	38.56	67.95	39.55	70.14	40.08	68.69	40.66
63	67.10	41.70	68.13	39.69	66.86	40.66	69.64	41.48	67.41	41.78
66	65.80	42.90	67.59	40.94	65.91	41.77	68.54	42.61	66.26	43.17
69	64.50	44.30	66.65	42.34	64.73	43.00	67.99	44.01	65.23	44.97
72	63.20	45.80	65.84	44.28	63.68	44.51	66.60	45.97	64.13	46.76

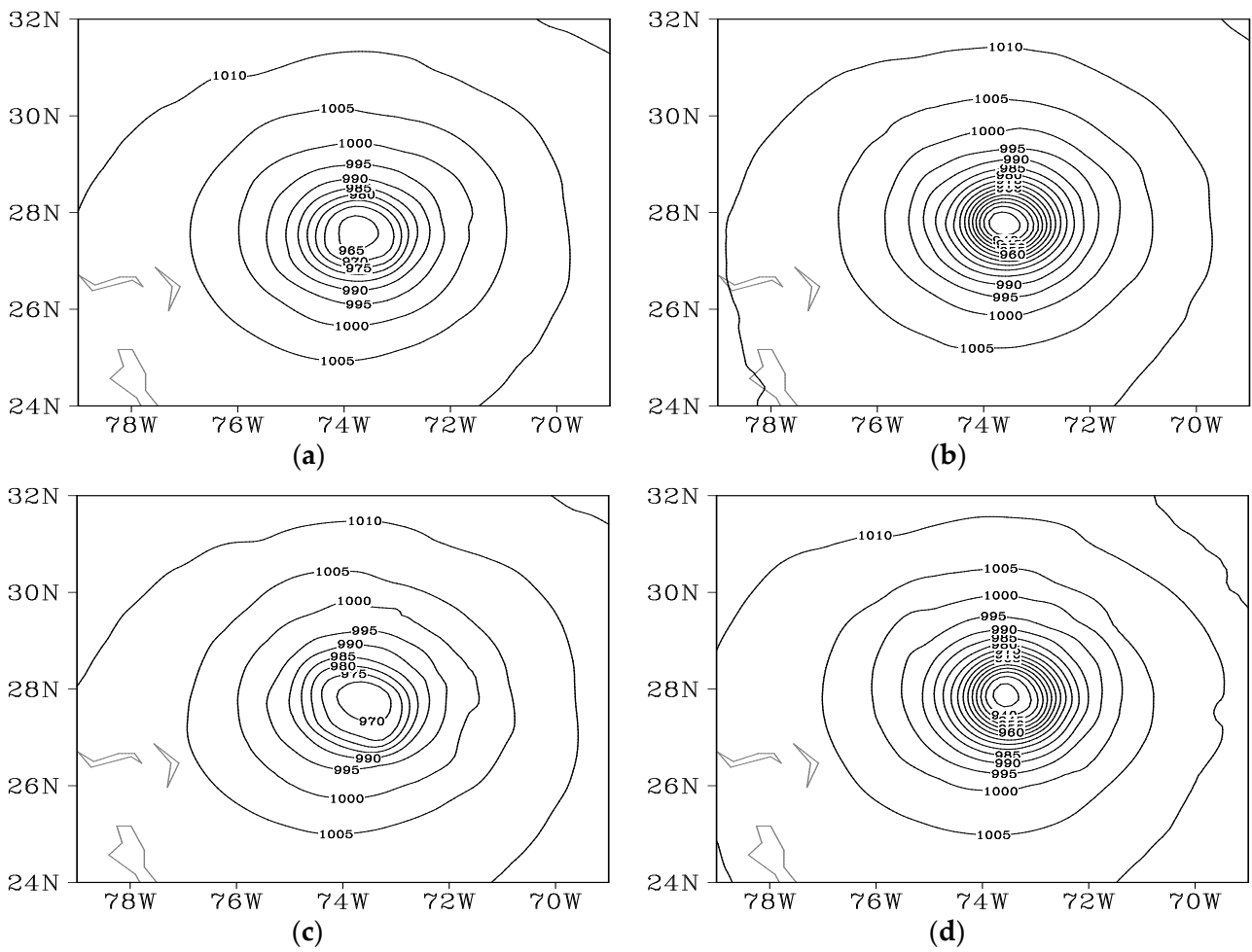


Figure A2. The spatial distribution of SLP at the 9 h mark of integration: (a) CTRL; (b) BDA; (c) SODA; (d) SOBDA. The SLP contour lines are spaced at intervals of 5 hPa.

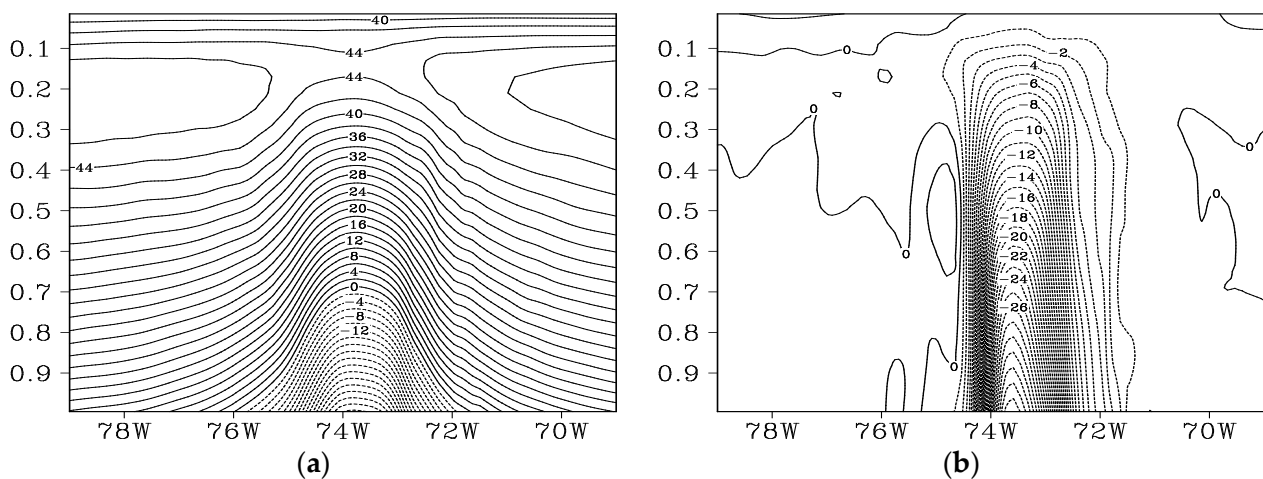


Figure A3. Cont.

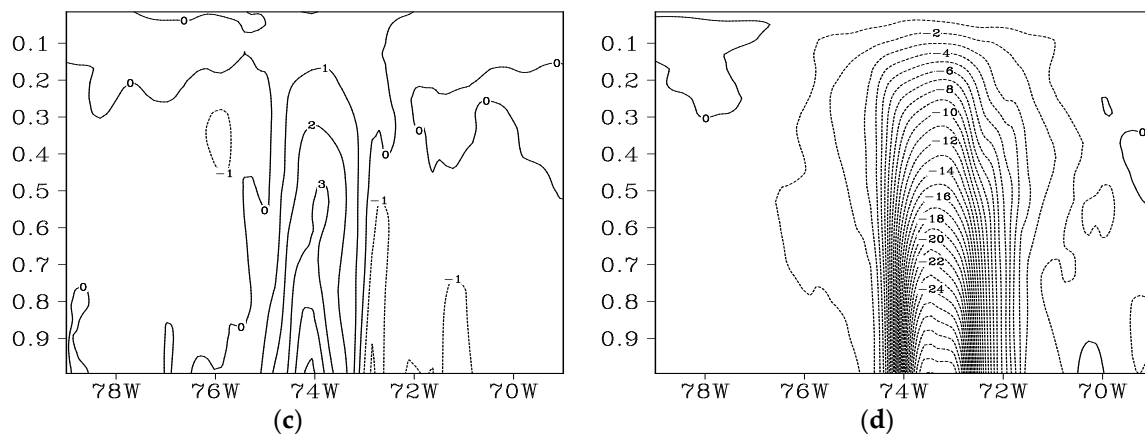


Figure A3. The cross-sectional view of pressure perturbation across the west–east axis prior to assimilation ((a) CTRL) and pressure perturbation increments after assimilation ((b) BDA; (c) SODA; (d) SOBDA) through the hurricane center at the 9 h mark of integration. The contour lines are spaced at different intervals: (a) 2 hPa; (b–d) 1 hPa.

References

1. Normand, C. Atmospheric ozone and the upper-air conditions. *Q. J. R. Meteorol. Soc.* **1953**, *79*, 39–50. [[CrossRef](#)]
2. Ohring, G.; Muench, H.S. Relationships between ozone and meteorological parameters in the lower stratosphere. *J. Atmos. Sci.* **1960**, *17*, 195–206. [[CrossRef](#)]
3. Danielsen, E.F. Stratospheric-tropospheric exchange based on radio-activity, ozone, and potential vorticity. *J. Atmos. Sci.* **1968**, *25*, 502–518. [[CrossRef](#)]
4. Shapiro, M.A.; Krueger, A.J.; Kennedy, P.J. Nowcasting the position and intensity of jet streams using a satellite-borne total ozone mapping spectrometer. In *Nowcasting*; Browning, K., Ed.; Academic Press: Cambridge, MA, USA, 1982; pp. 137–145.
5. Stout, J.; Rodgers, E.B. Nimbus-7 total ozone observations of western North Pacific tropical cyclones. *J. Appl. Meteorol. Climatol.* **1992**, *31*, 758–783. [[CrossRef](#)]
6. Riishøjgaard, L.P.; Källén, E. On the correlation between ozone and potential vorticity for large-scale Rossby waves. *J. Geophys. Res.* **1997**, *102*, 8793–8804. [[CrossRef](#)]
7. Davis, C.; Low-Nam, S.; Shapiro, M.A.; Zou, X.; Krueger, A.J. Direct retrieval of wind from Total Ozone Mapping Spectrometer (TOMS) data: Examples from FASTEX. *Q. J. R. Meteorol. Soc.* **1999**, *125*, 3375–3391. [[CrossRef](#)]
8. Jiang, X.; Pawson, S.; Camp, C.; Nielsen, J.E.; Shia, R.-L.; Liao, T.; Limpasuvan, V.; Yung, Y.L. Interannual variability and trends of extratropical ozone. Part I: Northern Hemisphere. *J. Atmos. Sci.* **2008**, *65*, 3013–3029. [[CrossRef](#)]
9. Carsey, T.P.; Willoughby, H.E. Ozone measurements from eyewall transects of two Atlantic tropical cyclones. *Mon. Weather Rev.* **2005**, *133*, 166–174. [[CrossRef](#)]
10. Zou, X.; Wu, Y. On the relationship between Total Ozone Mapping Spectrometer (TOMS) ozone and hurricanes. *J. Geophys. Res.* **2005**, *110*, D06109. [[CrossRef](#)]
11. Jang, K.I.; Zou, X.; De Pondecia, M.S.F.V.; Shapiro, M.; Davis, C.; Krueger, A. Incorporating TOMS ozone measurements into the prediction of the Washington, D.C., winter storm during 24–25 January 2000. *J. Appl. Meteorol. Climatol.* **2003**, *42*, 797–812. [[CrossRef](#)]
12. Wu, Y.; Zou, X. Numerical test of a simple approach for using TOMS total ozone data in hurricane environment. *Q. J. R. Meteorol. Soc.* **2008**, *134*, 1397–1408. [[CrossRef](#)]
13. Liu, Y.; Zou, X. Impact of 4DVAR assimilation of AIRS total column ozone observations on the simulation of Hurricane Earl. *J. Meteorol. Res.* **2015**, *29*, 257–271. [[CrossRef](#)]
14. Zou, X.; Xiao, Q. Studies on the initialization and simulation of a mature hurricane using a variational bogus data assimilation scheme. *J. Atmos. Sci.* **2000**, *57*, 836–860. [[CrossRef](#)]
15. Xiao, Q.; Zou, X.; Wang, B. Initialization and simulation of a landfalling hurricane using a variational bogus data assimilation scheme. *Mon. Weather Rev.* **2000**, *128*, 2252–2269. [[CrossRef](#)]
16. Zhao, Y.; Wang, B.; Wang, Y. Initialization and simulation of a landfalling typhoon using a variational bogus mapped data assimilation (BMDA). *Meteorol. Atmos. Phys.* **2007**, *98*, 269–282. [[CrossRef](#)]
17. Xiao, Q.; Chen, L.; Zhang, X. Evaluations of BDA scheme using the Advanced Research WRF (ARW) model. *J. Appl. Meteorol. Climatol.* **2009**, *48*, 680–689. [[CrossRef](#)]
18. Park, K.; Zou, X. Toward developing an objective 4DVAR BDA scheme for hurricane initialization based on TPC observed parameters. *Mon. Weather Rev.* **2004**, *132*, 2054–2069. [[CrossRef](#)]
19. Zou, X.; Xiao, Q.; Lipton, A.E.; Modica, G.D. A numerical study of the effect of GOES sounder cloud-cleared brightness temperatures on the prediction of Hurricane Felix. *J. Appl. Meteorol. Climatol.* **2001**, *40*, 34–55. [[CrossRef](#)]

20. Pu, Z.; Tao, W.-K.; Braun, S.; Simpson, J.; Jia, Y.; Halverson, J.; Olson, W.; Hou, A. The impact of TRMM data on mesoscale numerical simulation of Supertyphoon Paka. *Mon. Weather Rev.* **2002**, *130*, 2448–2458. [[CrossRef](#)]
21. Amerault, C.; Zou, X. Preliminary steps in assimilating SSM/I brightness temperatures in a hurricane prediction scheme. *J. Atmos. Ocean. Technol.* **2003**, *20*, 1154–1169. [[CrossRef](#)]
22. Zhao, Y.; Wang, B.; Ji, Z.; Liang, X.; Deng, G.; Zhang, X. Improved track forecasting of a typhoon reaching landfall from four-dimensional variational data assimilation of AMSU-A retrieved data. *J. Geophys. Res.* **2005**, *110*, D14101. [[CrossRef](#)]
23. Zhang, X.; Xiao, Q.; Fitzpatrick, P.J. The impact of multisatellite data on the initialization and simulation of Hurricane Lili's (2002) rapid weakening phase. *Mon. Weather Rev.* **2007**, *135*, 526–548. [[CrossRef](#)]
24. Wang, Y.; Wang, B.; Fei, J.; Han, Y.; Ma, G. The effects of assimilating satellite brightness temperature and bogus data on the simulation of Typhoon Kalmaegi (2008). *J. Meteorol. Res.* **2013**, *27*, 415–434. [[CrossRef](#)]
25. Liu, Y.; Zhang, W. Improved hurricane forecasting from a variational bogus and ozone data assimilation (BODA) scheme: Case study. *Meteorol. Atmos. Phys.* **2016**, *128*, 715–732. [[CrossRef](#)]
26. Gong, Y.; Liang, K.; Wu, X.; Shao, Q.; Li, W.; Liu, S.; Han, G.; Liu, H. An application of the A-4DEnVar to coupled parameter optimization. *Acta Oceanol. Sin.* **2022**, *41*, 60–70. [[CrossRef](#)]
27. Liang, K.; Li, W.; Han, G.; Shao, Q.; Zhang, X.; Zhang, L.; Jia, B.; Bai, Y.; Liu, S.; Gong, Y. An analytical four-dimensional ensemble-variational data assimilation scheme. *J. Adv. Model. Earth Syst.* **2021**, *13*, e2020MS002314. [[CrossRef](#)]
28. Fairbairn, D.; Pring, S.R.; Lorenc, A.C.; Roulstone, I. A comparison of 4DVar with ensemble data assimilation methods. *Q. J. R. Meteorol. Soc.* **2014**, *140*, 281–294. [[CrossRef](#)]
29. Arbogast, É.; Desroziers, G.; Berre, L. A parallel implementation of a 4DEnVar ensemble. *Q. J. R. Meteorol. Soc.* **2017**, *143*, 2073–2083. [[CrossRef](#)]
30. Yang, Y.; Mémin, E. High-resolution data assimilation through stochastic subgrid tensor and parameter estimation from 4DEnVar. *Tellus A* **2017**, *69*, 1308772. [[CrossRef](#)]
31. Song, H.J.; Kang, J.H. Effects of the wind-mass balance constraint on ensemble forecasts in the hybrid-4DEnVar. *Q. J. R. Meteorol. Soc.* **2019**, *145*, 434–449. [[CrossRef](#)]
32. Han, G.; Wu, X.; Zhang, S.; Liu, Z.; Navon, I.M.; Li, W. A study of coupling parameter estimation implemented by 4D-Var and EnKF with a simple coupled system. *Adv. Meteorol.* **2015**, *2015*, 530764. [[CrossRef](#)]
33. Tian, X.; Feng, X. A non-linear least squares enhanced POD-4DVar algorithm for data assimilation. *Tellus A* **2015**, *67*, 25340. [[CrossRef](#)]
34. Tian, X.; Zhang, H.; Feng, X.; Xie, Y. Nonlinear least squares En4DVar to 4DEnVar methods for data assimilation: Formulation, analysis, and preliminary evaluation. *Mon. Weather Rev.* **2018**, *146*, 77–93. [[CrossRef](#)]
35. Bian, J.; Gettelman, A.; Chen, H.; Pan, L.L. Validation of satellite ozone profile retrievals using Beijing ozonesonde data. *J. Geophys. Res.* **2007**, *112*, D06305. [[CrossRef](#)]
36. Monahan, K.P.; Pan, L.L.; McDonald, A.J.; Bodeker, G.E.; Wei, J.; George, S.E.; Barnett, C.D.; Maddy, E. Validation of AIRS v4 ozone profiles in the UTLS using ozonesondes from Lauder, NZ and Boulder, USA. *J. Geophys. Res.* **2007**, *112*, D17304. [[CrossRef](#)]
37. Pan, L.L.; Bowman, K.P.; Shapiro, M.; Randel, W.J.; Gao, R.S.; Campos, T.; Davis, C.; Schauffler, S.; Ridley, B.A.; Wei, J.C.; et al. Chemical behavior of the tropopause observed during the Stratosphere-Troposphere Analyses of Regional Transport experiment. *J. Geophys. Res.* **2007**, *112*, D18110. [[CrossRef](#)]
38. Pittman, J.V.; Pan, L.L.; Wei, J.C.; Irion, F.W.; Liu, X.; Maddy, E.S.; Barnett, C.D.; Chance, K.; Gao, R.-S. Evaluation of AIRS, IASI, and OMI ozone profile retrievals in the extratropical tropopause region using in situ aircraft measurements. *J. Geophys. Res.* **2009**, *114*, D24109. [[CrossRef](#)]
39. Zhao, H.; Shu, Y.; Mao, Y.; Liu, Y.; Yu, K. The Assimilation Effect of Multi-New Types Observation Data in the Forecasts of Meiyu-Front Rainstorm. *Atmosphere* **2023**, *14*, 693. [[CrossRef](#)]
40. Shu, A.; Shen, F.; Jiang, L.; Zhang, T.; Xu, D. Assimilation of Clear-sky FY-4A AGRI radiances within the WRFDA system for the prediction of a landfalling Typhoon Hagupit (2020). *Atmos. Res.* **2023**, *283*, 106556. [[CrossRef](#)]
41. Rodgers, E.B.; Stout, J.; Steranka, J.; Chang, S. Tropical cyclone-upper atmospheric interaction as inferred from satellite total ozone observations. *J. Appl. Meteorol. Climatol.* **1990**, *29*, 934–954. [[CrossRef](#)]
42. Bosart, L.F. Tropopause folding: Upper-level frontogenesis and beyond. In *A Half Century of Progress in Meteorology: A Tribute to Richard Reed*; Springer: Berlin/Heidelberg, Germany, 2003; pp. 13–47.
43. Song, L.; Shen, F.; Shao, C.; Shu, A.; Zhu, L. Impacts of 3DEnVar-Based FY-3D MWHS-2 Radiance Assimilation on Numerical Simulations of Landfalling Typhoon Ampil (2018). *Remote Sens.* **2022**, *14*, 6037. [[CrossRef](#)]
44. Qing, Z.; Zeng, Q.; Wang, H.; Liu, Y.; Xiong, T.; Zhang, S. ADASYN-LOF Algorithm for Imbalanced Tornado Samples. *Atmosphere* **2022**, *13*, 544. [[CrossRef](#)]
45. Liu, Y.; Zou, X. Quality control of AIRS total column ozone data within tropical cyclones. *Front. Earth Sci.* **2016**, *10*, 222–235. [[CrossRef](#)]
46. Fujita, T. Pressure distribution within a typhoon. *Geophys. Mag.* **1952**, *23*, 437–451.
47. Grell, G.A.; Dudhia, J.; Stauffer, D.R. A Description of the Fifth Generation Penn State/NCAR Mesoscale Model (MM5). In *NCAR Technical Note*; NCAR: Boulder, CO, USA, 1994; p. 117.
48. Dong, K.; Neumann, C.J. On the relative motion of binary tropical cyclones. *Mon. Weather Rev.* **1983**, *111*, 945–953. [[CrossRef](#)]

49. Velden, C.S.; Leslie, L.M. The basic relationship between tropical cyclone intensity and the depth of the environmental steering layer in the Australian region. *Weather Forecast.* **1991**, *6*, 244–253. [[CrossRef](#)]
50. Holland, G.J. Tropical cyclone motion: A comparison of theory and observation. *J. Atmos. Sci.* **1984**, *41*, 68–75. [[CrossRef](#)]
51. Wang, B.; Elsberry, R.L.; Wang, Y.; Wu, L. Dynamics in tropical cyclone motion: A review. *Chin. J. Atmos. Sci.* **1998**, *22*, 535–547. (In Chinese)

Disclaimer/Publisher’s Note: The statements, opinions and data contained in all publications are solely those of the individual author(s) and contributor(s) and not of MDPI and/or the editor(s). MDPI and/or the editor(s) disclaim responsibility for any injury to people or property resulting from any ideas, methods, instructions or products referred to in the content.